Upper critical field and its anisotropy in $RbCr_3As_3$

Qimei Liang,[1,2] Tong Liu,[3,4] Chuanying Xi,[1] Yuyan Han,[1] Gang Mu,[5,6] Li Pi,[1] Zhi-An Ren,[3,4,*] and Zhaosheng Wang[1,†]

[1]*Anhui Province Key Laboratory of Condensed Matter Physics at Extreme Conditions, High Magnetic Field Laboratory of the Chinese Academy of Sciences, Hefei 230031, China*

[2]*University of Science and Technology of China, Hefei 230026, China*

[3]*Beijing National Laboratory for Condensed Matter Physics, Institute of Physics, Chinese Academy of Sciences, Beijing 100190, China*

[4]*School of Physical Sciences, University of Chinese Academy of Sciences, Beijing 100049, China*

[5]*State Key Laboratory of Functional Materials for Informatics, Shanghai Institute of Microsystem and Information Technology, Chinese Academy of Sciences, Shanghai 200050, China*

[6]*CAS Center for Excellence in Superconducting Electronics(CENSE), Shanghai 200050, China*

(Received 9 September 2019; revised manuscript received 23 October 2019; published 23 December 2019)

The temperature dependence of the upper critical field (H_{c2}) in $RbCr_3As_3$ single crystals ($T_c \approx 7.3$ K) has been determined by means of magnetoresistance measurements with temperature down to 0.35 K in static magnetic fields up to 38 T. The magnetic field was applied both for directions parallel ($H \parallel c$, $H_{c2}^{\parallel c}$) and perpendicular ($H \perp c$, $H_{c2}^{\perp c}$) to the Cr chains. The curves $H_{c2}^{\parallel c}(T)$ and $H_{c2}^{\perp c}(T)$ cross at ~5.5 K. As a result, the anisotropy parameter $\gamma(T) = H_{c2}^{\perp c}/H_{c2}^{\parallel c}(T)$ increases from 0.5 near T_c to 1.6 at low temperature. Fitting with the Werthamer-Helfand-Hohenberg (WHH) model yields zero-temperature critical fields of $\mu_0 H_{c2}^{\parallel c}(0) \approx 27.2$ T and $\mu_0 H_{c2}^{\perp c}(0) \approx 43.4$ T, both exceeding the BCS weak-coupling Pauli limit $\mu_0 H_p = 1.84 T_c = 13.4$ T. The results indicate that the paramagnetic pair-breaking effect is strong for $H \parallel c$ but absent for $H \perp c$, which was further confirmed by the angle dependent magnetoresistance and H_{c2} measurements.

DOI: 10.1103/PhysRevB.100.214512

I. INTRODUCTION

Recently, superconductivity was found in Cr-based ternary compounds $A_2Cr_3As_3$ at ambient pressure [1–4] following the discovery of superconductivity in CrAs at a critical pressure $P_c \approx 8$ kbar [5]. $A_2Cr_3As_3$ compounds have a quasi-one-dimensional (Q1D) hexagonal noncentrosymmetric crystal structure with a space group of $P\bar{6}m2$. The infinite $[(Cr_3As_3)^{2-}]_\infty$ linear chains are separated by alkali-metal cations. For A = Na, K, Rb, and Cs, the superconducting T_c is 8.6, 6.1, 4.8, and 2.2 K, respectively [1–4]. As showing very particular crystal structure and unconventional superconducting properties, this Cr-based superconducting family has attracted intense interests [6–19]. However, the experimental results within the context of pairing symmetry have not yet reached a consensus [20,21]. $A_2Cr_3As_3$ superconductors are extremely reactive when exposed in air, probably due to the existence of crowded A1 atoms in the crystal structure [1]. The samples are easily oxidized during most experimental procedures, which hinders many further studies for their intrinsic physical characteristics.

Lately, by deintercalating half of the A^+ ions using ethanol from the $A_2Cr_3As_3$ lattice, another type of Q1D compounds ACr_3As_3 (A = K, Rb, Cs) with similar crystal structure were obtained, with $T_c \approx 5$ and 7.3 K for KCr_3As_3 and $RbCr_3As_3$ [22,23]. Unlike the $A_2Cr_3As_3$ compounds, ACr_3As_3 superconductors have a centrosymmetric lattice with the space group $P6_3/m$ and are air stable [21–23]. Recent neutron and x-ray diffraction measurements show that the superconductivity in KCr_3As_3 is induced by hydrogen doping [24]. Density functional theory (DFT) analysis shows that $KH_xCr_3As_3$ has a similar electronic structure to $K_2Cr_3As_3$ [24]. Thus it is important to study the superconducting properties of ACr_3As_3 and compare to the $A_2Cr_3As_3$ compounds. As a basic parameter, the temperature dependence of the upper critical field H_{c2} reflects the underlying electronic structure responsible for superconductivity and provides valuable information on the microscopic origin of pair breaking. By measuring the temperature dependence of H_{c2} of $RbCr_3As_3$, information on the superconducting pairing mechanism of ACr_3As_3 superconductors can be gained.

In this work we present temperature and magnetic field dependent magnetoresistance measurements with magnetic fields applied parallel and perpendicular to the c axis, and angle dependent magnetoresistance measurements on $RbCr_3As_3$ single crystals. H_{c2} was determined over a wide range of temperatures down to 0.35 K in static magnetic fields up to 38 T. We find that the curves $H_{c2}^{\parallel c}(T)$ and $H_{c2}^{\perp c}(T)$ cross at ~5.5 K, and both $H_{c2}^{\parallel c}(0)$ and $H_{c2}^{\perp c}(0)$ exceed the BCS weak-coupling Pauli limit. The results indicate that the paramagnetic pair-breaking effect is strong for $H \parallel c$ but absent for $H \perp c$, which was further confirmed by the angle dependent magnetoresistance and H_{c2} measurements.

II. EXPERIMENT

Single crystals of $RbCr_3As_3$ were prepared by the deintercalation of Rb^+ ions from $Rb_2Cr_3As_3$ precursors, which were

*renzhian@iphy.ac.cn
†zswang@hmfl.ac.cn

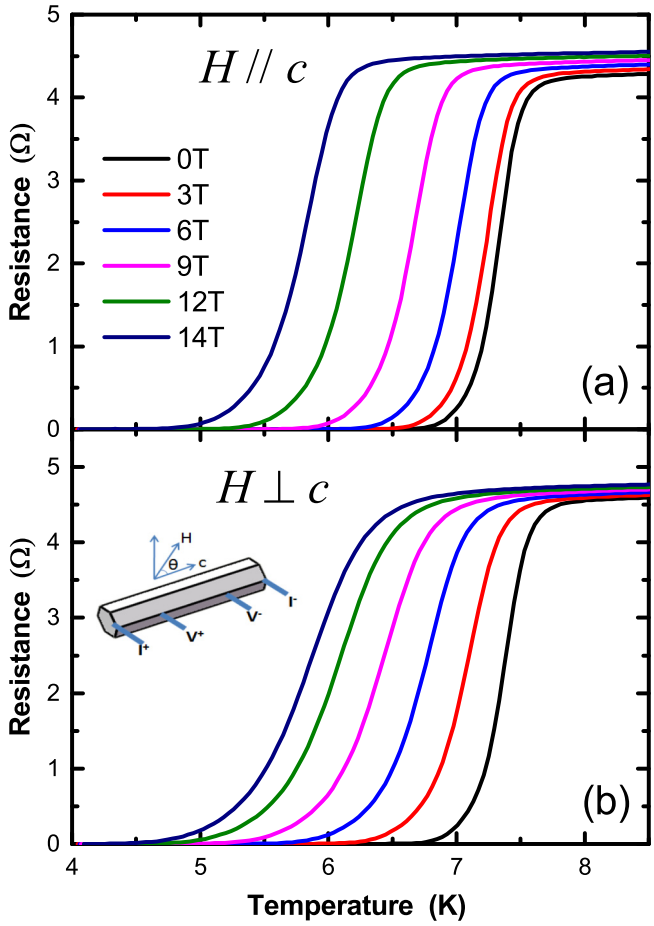

FIG. 1. Temperature dependence of resistance for $RbCr_3As_3$ single crystal A1 at fields $\mu_0 H = 0$, 3, 6, 9, 12, and 14 T with (a) $H \parallel c$ and (b) $H \perp c$, respectively. The inset of (b) illustrates the definition of angle θ.

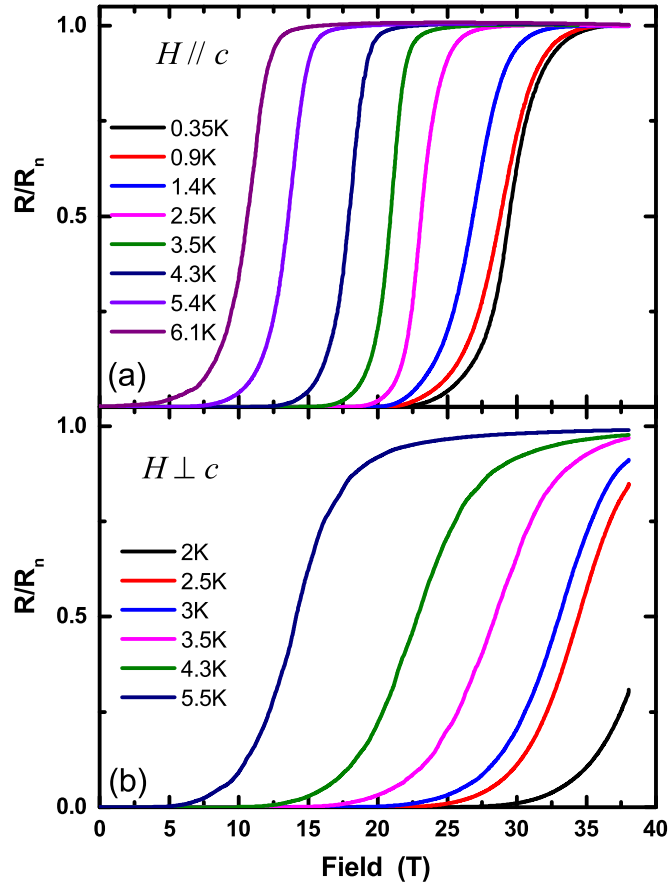

FIG. 2. Magnetic field dependence of resistance for $RbCr_3As_3$ single crystal A1 at different temperatures with (a) $H \parallel c$ and (b) $H \perp c$ up to 38 T. The data are normalized to the value in the normal state R_n (the resistance at 6.1 K and 38 T).

grown out of the RbAs and CrAs mixture using a high temperature solution growth method [25]. The as-grown $Rb_2Cr_3As_3$ single crystals were immersed in pure dehydrated ethanol and kept for one week for the fully deintercalation of Rb^+ ions at room temperature. The obtained samples were washed by ethanol thoroughly. To further improve the sample quality, the as-prepared crystals were annealed in an evacuated quartz tube at 373 K for 10 h [22]. All the experimental procedures were performed in a glove box filled with high-purity Ar gas to avoid introducing impurities. More detailed information can be found in Ref. [23]. The obtained $RbCr_3As_3$ crystals are needlelike with a typical size of $5 \times 0.2 \times 0.18$ mm^3, and quite stable in air at room temperature.

The resistance was measured by a standard four-probe method with a current $I = 100$ μA flowing along the c axis [as shown in the inset of Fig. 1(b)]. Magnetic fields were applied parallel and perpendicular to the c axis ($H \parallel c$, $H \parallel I$ and $H \perp c$, $H \perp I$). The temperature and angular dependence of resistance was measured by use of a commercial Physical Property Measurement System (PPMS) with magnetic fields up to 14 T. In the angle dependent measurements, $\theta = 0^\circ$ corresponded to the configuration of $H \parallel c$ axis and $\theta = 90^\circ$ to $H \perp c$ axis, respectively. The field dependent resistance measurements shown in Fig. 2 were carried out at temperatures down to 0.35 K with a ^{3}He cryostat in the High Magnetic Field Laboratory of Chinese Academy of Science. A water-cooling magnet which generates the maximum magnetic field up to 38.5 T was employed. The samples were fixed on the sample holder with GE-7031 varnish. A delta mode system with Keithley models 6221 and 2182A was used.

III. RESULTS AND DISCUSSION

We measured five $RbCr_3As_3$ samples from two batches (labeled as A1, A2, A3 and B1, B2). All samples show similar behaviors. Figure 1 shows a typical result of the temperature dependent resistance in magnetic fields from 0 to 14 T for $H \parallel c$ and $H \perp c$, respectively. The magnetic field shifts the zero-resistance state to lower temperature a bit slower for $H \parallel c$ than for $H \perp c$ at a temperature close to T_c. As the temperature decreases, the case is reversed, which implies a reversal of the anisotropy of H_{c2}.

The magnetic field dependent resistances measured at different temperatures in static magnetic fields up to 38 T for $H \parallel c$ and $H \perp c$ are shown in Figs. 2(a) and 2(b), respectively. The sample is the same one shown in Fig. 1. Apparently, 38 T is enough to suppress superconductivity completely at temperatures down to 0.35 K for $H \parallel c$. However, a stronger

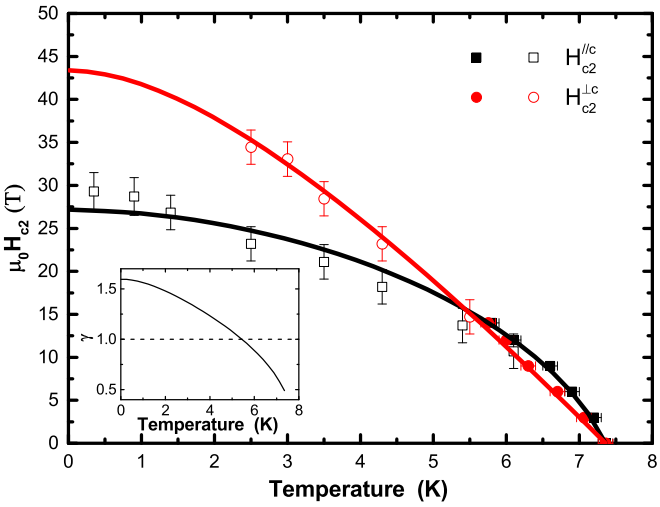

FIG. 3. Temperature dependence of H_{c2} extracted from the magnetoresistance measurements for $RbCr_3As_3$ single crystal A1. The solid symbols are obtained from PPMS measurements, and the open symbols are obtained from water-cooling magnet measurements. The black and red solid lines show WHH fits for $H_{c2}^{\|c}$ and $H_{c2}^{\perp c}$ with fitting parameters $\alpha = 8$, $\lambda_{so} = 1.6$ and $\alpha = 0$, $\lambda_{so} = 0$, respectively. The inset shows the anisotropy parameter $\gamma(T)$ calculated from the fitting results.

field is needed to suppress superconductivity for $H \perp c$ at low temperatures. Thus a reversal of the anisotropy of H_{c2} has been confirmed. As the current flowed along the c axis during the measurements, it was Lorentz force free for $H \| c$. However, for $H \perp c$, there was a maximum of Lorentz force, which could generate a motion of the vortices and lead to a finite resistance region [26]. This region is called the vortex-liquid phase, which broadens the resistive transitions [27]. As shown in Figs. 1 and 2, field-induced broadenings of the resistive transitions are small, suggesting a very narrow vortex-liquid region in $RbCr_3As_3$. This behavior is similar to $A_2Cr_3As_3$ compounds [11–14] and some Fe-based superconductors like Ba122 [28–31], $FeTe_{0.6}Se_{0.4}$ [32], and LiFeAs [33]. In order to reduce the influence of the vortex-liquid phase and superconducting fluctuations, the temperature or field where the normal-state resistance R_n is reduced to 50% was chosen as the criterion to determine the H_{c2}-T phase diagram.

The resulting critical fields $H_{c2}^{\|c}$ and $H_{c2}^{\perp c}$ are summarized in Fig. 3. The closed symbols are obtained from PPMS measurements by use of temperature scans, and the open symbols are obtained from water-cooling magnet measurements utilizing magnetic field scans. The slopes $\mu_0 H' = \mu_0 dH_{c2}^{c}/dT_c$ at T_c are -18 and -8.5 T/K for $H \| c$ and $H \perp c$, respectively. According to the Ginzburg-Landau (GL) theory, the effective mass anisotropy $m_\perp/m_\| = (H_{c2}^{\|c'}/H_{c2}^{\perp c'})^2 \approx 4.5$. This anisotropy value is only about one-sixth of that in $Rb_2Cr_3As_3$ [14], revealing an reduced Q1D character in $RbCr_3As_3$. According to the Werthamer-Helfand-Hohenberg (WHH) formula [34], $H_{c2}^{orb} = -0.73 T_c (dH_{c2}/dT)\,|_{T_c}$. Using the GL relations $H_{c2}^{orb,\|c}(0) = \Phi_0/(2\pi\xi_{\perp c}^2)$ and $H_{c2}^{orb,\perp c}(0) = \Phi_0/(2\pi\xi_{\perp c}\xi_{\|c})$, where Φ_0 is the magnetic flux quantum, the anisotropic coherence lengths can be estimated as $\xi_{\perp c}(0) \approx 1.9$ nm and $\xi_{\|c}(0) \approx 3.9$ nm, respectively. These values are close to the results reported in $Rb_2Cr_3As_3$ [14]. The $\xi_{\perp c}(0)$ value is about twice of the interchain distance [23], indicating a uniaxially anisotropic 3D superconductivity. As temperature decreases, the curves $H_{c2}^{\|c}(T)$ and $H_{c2}^{\perp c}(T)$ cross at $T \approx 5.5$ K. For a weak coupling conventional BCS superconductor, the Pauli-limiting field can be estimated by [35] $\mu_0 H_p = 1.84 T_c$ T, resulting in $\mu_0 H_p = 13.4$ T. From Fig. 3 one can see $H_{c2}^{\|c}(0)$ and $H_{c2}^{\perp c}(0)$ are larger than the Pauli limiting by two and three times, respectively. These results are similar to the results of $A_2Cr_3As_3$ [11–14], indicating comparable strong electron correlation in the Cr-based family.

To quantitatively describe our results, we use the full WHH formula that incorporates the spin-paramagnetic effect via the Maki parameter α and the spin-orbit scattering constant λ_{so} to describe the experimental $H_{c2}(T)$ data [34]:

$$\ln\frac{1}{t} = \sum_{\nu=-\infty}^{\infty}\left\{\frac{1}{|2\nu+1|} - \left[|2\nu+1| + \frac{\bar{h}}{t} + \frac{(\alpha\bar{h}/t)^2}{|2\nu+1| + (\bar{h}+\lambda_{so})/t}\right]^{-1}\right\}, \quad (1)$$

where $t = T/T_c$ and $\bar{h} = (4/\pi^2)[H_{c2}/|dH_{c2}/dT|_{T_c}]$. As shown by the solid line in Fig. 3, the best fit ($\alpha = 8$, $\lambda_{so} = 1.6$ and $\alpha = 0$, $\lambda_{so} = 0$) can reproduce the experimental data well, resulting in $\mu_0 H_{c2}^{\|c}(0) = 27.2$ T and $\mu_0 H_{c2}^{\perp c}(0) = 43.4$ T, respectively. The results indicate that Pauli pair breaking is strong for $H_{c2}^{\|c}(T)$ but absent for $H_{c2}^{\perp c}(T)$. As $\alpha \propto \gamma_n \rho_n$ [34], where γ_n and ρ_n are the normal state electronic specific heat coefficient and the normal state DC resistivity respectively, the large α is consistent with the high γ_n and ρ_n reported in the ACr_3As_3 compounds [22,36]. According to the Maki formula [37], for $H \| c$, $\alpha = \sqrt{2} H_{c2}^{orb,\|c}(0)/H_p = 10$. The fitting result is a bit smaller than the value calculated from the Maki formula. This deviation has been widely observed in Fe-based superconductors, and been considered to be a consequence of the enhancement of H_p over H_p^{BCS} due to the strong coupling effect [38].

The anisotropy parameter $\gamma(T) = H_{c2}^{\perp c}/H_{c2}^{\|c}(T)$ can be calculated from the fitting results. γ increases from 0.5 near T_c to >1 below $T \approx 5.5$ K where the $H_{c2}(T)$ curves cross, and about 1.6 at low temperature. Similar behaviors of γ have been reported in $A_2Cr_3As_3$ [11,13,14], heavy-fermion superconductor UPt_3 [39], and Q1D superconductors $Li_{0.9}Mo_6O_7$ [40] and organic superconductors $(TMTSF)_2PF_6$ [41]. Recently, DFT calculations find strong structural instabilities of KCr_3As_3, which would lead to a much more one-dimensional Fermi surface structure [42]. However, comparing to $\gamma = 0.19$ near T_c in $Rb_2Cr_3As_3$ [14], $\gamma = 0.5$ clearly indicates weaker anisotropy in $RbCr_3As_3$ which possesses smaller interchain distance.

According to the anisotropic Ginzburg-Landau theory, the effective-mass anisotropy leads to the anisotropy of the orbital limited upper critical field $H_{c2}^{GL}(\theta) = H_{c2}^{\|c}/\sqrt{\cos^2(\theta) + \gamma^{-2}\sin^2(\theta)}$, and the resistivity in the mixed state depends on the effective field $H/H_{c2}^{GL}(\theta)$ [43]. Thus the maximum and minimum of the angle dependent resistance should be at $\theta = 0°$ or 90° depending on γ >1 or <1.

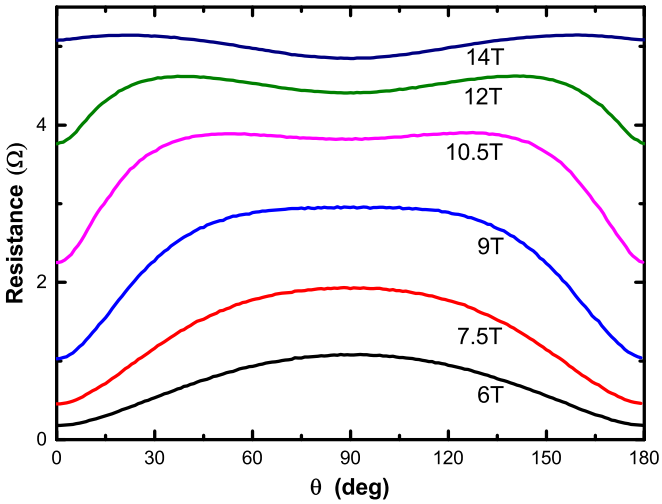

FIG. 4. Angular dependence of resistance at 6.5 K with magnetic field $\mu_0 H = 6$, 7.5, 9, 10.5, 12, and 14 T for $RbCr_3As_3$ single crystal A2.

Figure 4 presents angle dependent resistance at 6.5 K for $RbCr_3As_3$ single crystal A2. When the magnetic field is less than 9 T, the maximum of the resistance is at $\theta = 90^\circ$. However, a hollow shows up at $\theta = 90^\circ$ as the magnetic field increases further, indicating that there is a strong anisotropic paramagnetic pair-breaking effect in this system. These results are consistent with the results shown in Fig. 3.

In order to check the angular dependence of H_{c2} directly, field dependent magnetoresistance measurements were done with different angles between the magnetic field and the c axis at 6 and 6.5 K. The results of $H_{c2}(\theta)$ of $RbCr_3As_3$ single crystal B1 are shown in Fig. 5. H_{c2} does not decrease monotonously as the field direction is tilted from $H \parallel c$ to $H \perp c$. Instead, a minimum appears between $\theta = 0^\circ$ and 90°, which is similar to what has been observed in $K_2Cr_3As_3$ [13]. To include the strong anisotropic paramagnetic pair-breaking

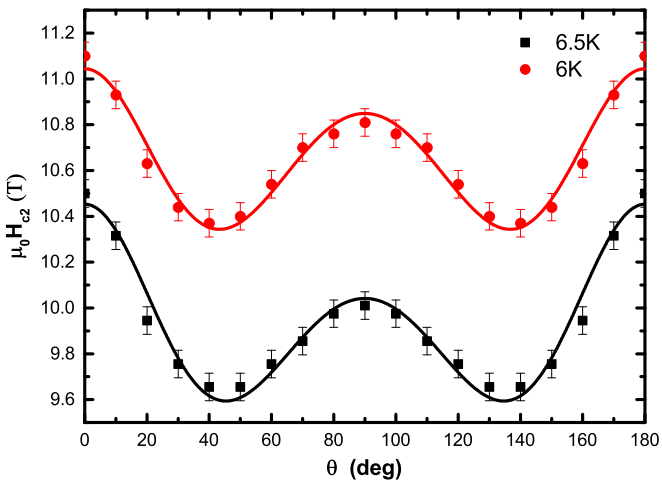

FIG. 5. Angular dependence of H_{c2} at 6 and 6.5 K for $RbCr_3As_3$ single crystal B1. The solid lines are the fitted data using Eqs. (2) with $\mu_0 H^{\rm orb}_{c2,\parallel} = 13.8$ T, $\gamma = 0.74$, $\mu_0 H^{\parallel}_{pm} = 8.8$ T for 6 K and $\mu_0 H^{\rm orb}_{c2,\parallel} = 13.7$ T, $\gamma = 0.73$, $\mu_0 H^{\parallel}_{pm} = 8.8$ T for 6.5 K, respectively.

effect, one can assume $H_{\rm pm}(\theta) = H^{\parallel}_{\rm pm} cos(\theta)$, where $H_{\rm pm}$ is an effective Pauli-limiting field. Thus $H_{\rm pm} = H^{\parallel}_{\rm pm}$ for $\theta = 0$, and $H_{\rm pm} = 0$ for $\theta = 90^\circ$. As $[H_{c2}(\theta)]^2 = [H^{\rm orb}_{c2}(\theta)]^2 - [H_{\rm pm}(\theta)]^2$ [13], one can get

$$H_{c2}(\theta) = \sqrt{\frac{(H^{\rm orb}_{c2,\parallel})^2}{\cos^2(\theta) + \gamma^{-2}\sin^2(\theta)}} - [H^{\parallel}_{\rm pm}\cos(\theta)]^2. \quad (2)$$

As shown in Fig. 5, the $H_{c2}(\theta)$ data can be fitted very well by the above equation, confirming the absence of Pauli-limiting effect for $\theta = 90^\circ$. Similar results have been reported in $K_2Cr_3As_3$ [11,13]. Usually the $H_{c2}(0)$ value is limited by paramagnetic effect regardless of field directions for a conventional superconductor with a high $H_{c2}(0)$ comparable to H_p. Regarding the insensitivity of T_c to nonmagnetic impurities and the behavior of $H_{c2}(T)$ in $K_2Cr_3As_3$, Balakirev *et al.* proposed a novel spin-singlet superconductivity with electron-spin locking along the c direction [11]. Zuo *et al.* pointed out that the spin state of $|\leftleftarrows> + |\rightrightarrows>$ is equivalent to $|\uparrow\downarrow> + |\downarrow\uparrow>$ with $S_z = 0$ for the odd-parity Cooper pairs [13]. For $H \parallel c$, the Zeeman energy breaks the Cooper pairs, showing the Pauli-limiting behavior. However, for $H \perp c$, the field simply changes the population of Cooper pairs with spin directions $|\leftleftarrows>$ and $|\rightrightarrows>$, and therefore no paramagnetic pair breaking is expected.

Until now, different paring mechanism and symmetry has been proposed for $A_2Cr_3As_3$ compounds, such as p_z-wave spin triplet [7,16,44], spin singlet [11,15], and a two-band model [45,46]. The experimental results have not yet reached a consensus [20,21]. The extremely air sensitivity property of $A_2Cr_3As_3$ hinders many further studies for their intrinsic physical characteristics. In Table I all the parameters of $RbCr_3As_3$ we have obtained are summarized and compared to $Rb_2Cr_3As_3$. Most of the parameters of the two compounds are close except $m_\perp/m_\parallel$, especially the ratio of $H_{c2}(0)/T_c$ (for both $H \parallel c$ and $H \perp c$) are almost the same. Although ACr_3As_3 has a centrosymmetric crystal structure differing from its noncentrosymmetric counterpart $A_2Cr_3As_3$, all of the results we obtained above indicate that the superconducting property of $RbCr_3As_3$ is very similar to the $Rb_2Cr_3As_3$ compounds. Investigations on the air stable ACr_3As_3 compound may provide a good path to acquire deep insight into the superconducting mechanism in the Q1D Cr-based family, and may help to expand the overall understanding of unconventional superconductivity.

IV. SUMMARY

In summary, we have constructed the H_{c2}-T phase diagram for $RbCr_3As_3$ with $T_c \approx 7.3$ K by use of magnetoresistance measurements with temperature down to 0.35 K in static magnetic fields up to 38 T both for directions parallel and perpendicular to the c axis. Fitting with the WHH model yields zero-temperature critical fields of $\mu_0 H^{\parallel c}_{c2}(0) \approx 27.2$ T and $\mu_0 H^{\perp c}_{c2}(0) \approx 43.4$ T, both exceeding the BCS weak-coupling Pauli limit. The anisotropy of H_{c2} has a reversal at ~5.5 K. The paramagnetic pair-breaking effect is strong for $H \parallel c$ but absent for $H \perp c$, which was further confirmed by the $H_{c2}(\theta)$ data.

TABLE I. Summary of the parameters of $RbCr_3As_3$ and $Rb_2Cr_3As_3$. The data of $Rb_2Cr_3As_3$ are from Ref. [14].

	T_c (K)	$\mu_0 H_{c2}^{\parallel c'}\|_{T_c}$ (T/K)	$\mu_0 H_{c2}^{\perp c'}\|_{T_c}$ (T/K)	$m_\perp/m_\parallel$	$\xi_{\parallel c}(0)$ (nm)	$\xi_{\perp c}(0)$ (nm)	$\mu_0 H_p$ (T)	$\mu_0 H_{c2}^{\parallel c}(0)$ (T)	$\mu_0 H_{c2}^{\perp c}(0)$ (T)	$\gamma(0)$	$\gamma(T_c)$	$T(\gamma=1)$ (K)
$RbCr_3As_3$	7.3	−18	−8.5	4.5	3.9	1.9	13.4	27.2	43.4	1.6	0.5	$0.75T_c$
$Rb_2Cr_3As_3$	4.8	−16	−3	28	3.2	2.1	8.8	17.5	29	1.7	0.19	$0.4T_c$

ACKNOWLEDGMENTS

This work was supported by the National Natural Science Foundation of China (Grants No. 11704385, No. 11874359, and No. 11774402). A portion of this work was performed on the Steady High Magnetic Field Facilities, High Magnetic Field Laboratory, Chinese Academy of Sciences, and supported by the High Magnetic Field Laboratory of Anhui Province.

[1] J. K. Bao, J. Y. Liu, C. W. Ma, Z. H. Meng, Z. T. Tang, Y. L. Sun, H. F. Zhai, H. Jiang, H. Bai, C. M. Feng, Z. A. Xu, and G. H. Cao, Phys. Rev. X **5**, 011013 (2015).

[2] Z. T. Tang, J. K. Bao, Y. Liu, Y. L. Sun, A. Ablimit, H. F. Zhai, H. Jiang, C. M. Feng, Z. A. Xu, and G. H. Cao, Phys. Rev. B **91**, 020506(R) (2015).

[3] Z. T. Tang, J. K. Bao, Z. Wang, H. Bai, H. Jiang, Y. Liu, H. F. Zhai, C. M. Feng, Z. A. Xu, and G. H. Cao, Sci. China Mater. **58**, 16 (2015).

[4] Q. G. Mu, B.-B. Ruan, B. J. Pan, T. Liu, J. Yu, K. Zhao, G. F. Chen, and Z. A. Ren, Phys. Rev. Mater. **2**, 034803 (2018).

[5] W. Wu, J. Cheng, K. Matsubayashi, P. Kong, F. Lin, C. Jin, N., Y. Uwatoko, and J. Luo, Nat. Commun. **5**, 5508 (2014).

[6] M. D. Watson, Y. Feng, C. W. Nicholson, C. Monney, J. M. Riley, H. Iwasawa, K. Refson, V. Sacksteder, D. T. Adroja, J. Zhao, and M. Hoesch, Phys. Rev. Lett. **118**, 097002 (2017).

[7] H. Zhong, X.-Y. Feng, H. Chen, and J. Dai, Phys. Rev. Lett. **115**, 227001 (2015).

[8] H. Z. Zhi, T. Imai, F. L. Ning, J.-K. Bao, and G.-H. Cao, Phys. Rev. Lett. **114**, 147004 (2015).

[9] G. M. Pang, M. Smidman, W. B. Jiang, J. K. Bao, Z. F. Weng, Y. F. Wang, L. Jiao, J. L. Zhang, G. H. Cao, and H. Q. Yuan, Phys. Rev. B **91**, 220502(R) (2015).

[10] J.-J. Miao, F.-C. Zhang, and Y. Zhou, Phys. Rev. B **94**, 205129 (2016).

[11] F. F. Balakirev, T. Kong, M. Jaime, R. D. McDonald, C. H. Mielke, A. Gurevich, P. C. Canfield, and S. L. Bud'ko, Phys. Rev. B **91**, 220505(R) (2015).

[12] T. Kong, S. L. Bud'ko, and P. C. Canfield, Phys. Rev. B **91**, 020507(R) (2015).

[13] H. Zuo, J.-K. Bao, Y. Liu, J. Wang, Z. Jin, Z. Xia, L. Li, Z. Xu, J. Kang, Z. Zhu, and G.-H. Cao, Phys. Rev. B **95**, 014502 (2017).

[14] Z.-T. Tang, Y. Liu, J.-K. Bao, C.-Y. Xi, L. Pi, and G.-H. Cao, J. Phys.: Condens. Matter **29**, 424002 (2017).

[15] A. Subedi, Phys. Rev. B **92**, 174501 (2015).

[16] X. Wu, F. Yang, C. Le, H. Fan, and J. Hu, Phys. Rev. B **92**, 104511 (2015).

[17] D. T. Adroja, A. Bhattacharyya, M. Telling, Yu Feng, M. Smidman, B. Pan, J. Zhao, A. D. Hillier, F. L. Pratt, and A. M. Strydom, Phys. Rev. B **92**, 134505 (2015).

[18] W. L. Zhang, H. Li, Dai Xia, H. W. Liu, Y. G. Shi, J. L. Luo, J. Hu, P. Richard, and H. Ding, Phys. Rev. B **92**, 060502(R) (2015).

[19] J. Luo, J. Yang, R. Zhou, Q. G. Mu, T. Liu, Z. Ren, C. J. Yi, Y. G. Shi, and G. Zheng, Phys. Rev. Lett. **123**, 047001 (2019).

[20] G.-H. Cao, J.-K. Bao, Z.-T. Tang, Y. Liu, and H. Jiang, Philos. Mag. **97**, 591 (2017).

[21] R. Y. Chen and N. L. Wang, Rep. Prog. Phys. **82**, 012503 (2019).

[22] Q. G. Mu, B.-B. Ruan, B. J. Pan, T. Liu, J. Yu, K. Zhao, G. F. Chen, and Z. A. Ren, Phys. Rev. B **96**, 140504(R) (2017).

[23] T. Liu, Q. G. Mu, B. J. Pan, J. Yu, B. B. Ruan, K. Zhao, G. F. Chen, and Z. A. Ren, Europhys. Lett. **120**, 27006 (2017).

[24] K. M. Taddei, L. D. Sanjeewa, B.-H. Lei, Y. Fu, Q. Zheng, D. J. Singh, A. S. Sefat, and C. dela Cruz, arXiv:1905.03360.

[25] P. C. Canfield and Z. Fisk, Philos. Mag. B **65**, 1117 (1992).

[26] L. P. Gor'kov and N. B. Kopnin, Usp. Fiz. Nauk **116**, 413 (1975).

[27] J. E. Sonier, J. H. Brewer, and R. F. Kiefl, Rev. Mod. Phys. **72**, 769 (2000).

[28] H. Yuan, J. Singleton, F. F. Balakirev, S. A. Baily, G. Chen, J. Luo, and N. Wang, Nature (London) **457**, 565 (2009).

[29] M. Kano, Y. Kohama, D. Graf, F. Balakirev, A. S. Sefat, M. A. Mcguire, B. C. Sales, D. Mandrus, and S. W. Tozer, J. Phys. Soc. Jpn. **78**, 084719 (2009).

[30] Z. S. Wang, H. Q. Luo, C. Ren, and H. H. Wen, Phys. Rev. B **78**, 140501(R) (2008).

[31] Z. Wang, T. Xie, E. Kampert, T. Förster, X. Lu, R. Zhang, D. Gong, S. Li, T. Herrmannsdörfer, J. Wosnitza, and H. Luo, Phys. Rev. B **92**, 174509 (2015).

[32] S. Khim, J. W. Kim, E. S. Choi, Y. Bang, M. Nohara, H. Takagi, and K. H. Kim, Phys. Rev. B **81**, 184511 (2010).

[33] S. Khim, B. Lee, J. W. Kim, E. S. Choi, G. R. Stewart, and K. H. Kim, Phys. Rev. B **84**, 104502 (2011).

[34] N. Werthamer, E. Helfand, and P. Hohenberg, Phys. Rev. **147**, 295 (1966).

[35] A. M. Clogston, Phys. Rev. Lett. **9**, 266 (1962).

[36] Q. Li, M. X. Wang, T. Liu, Q. G. Mu, Z. A. Ren, and S. Y. Li, Acta Phys. Sin. **67**, 207411 (2018).

[37] K. Maki, Phys. Phys. Fiz. **1**, 127 (1964).

[38] T. Wang, C. Zhang, L. Xu, J. Wang, S. Jiang, Z. Zhu, Z. Wang, J. Chu, J. Feng, L. Wang, W. Li, T. Hu, X. Liu, and G. Mu, Sci. China-Phys. Mech. Astron. **63**, 227412 (2020).

[39] G. R. Stewart, Z. Fisk, J. O. Willis, and J. L. Smith, Phys. Rev. Lett. **52**, 679 (1984).

[40] A. G. Lebed and O. Sepper, Phys. Rev. B **87**, 100511(R) (2013).

[41] I. J. Lee, M. J. Naughton, G. M. Danner, and P. M. Chaikin, Phys. Rev. Lett. **78**, 3555 (1997).
[42] G. Xing, L. Shang, Y. Fu, W. Ren, X. Fan, W. Zheng, and D. J. Singh, Phys. Rev. B **99**, 174508 (2019).
[43] G. Blatter, V. B. Geshkenbein, and A. I. Larkin, Phys. Rev. Lett. **68**, 875 (1992).
[44] Y. Zhou, C. Cao, and F.-C. Zhang, Sci. Bull. **62**, 208 (2017).
[45] G. Wachtel and Y. B. Kim, Phys. Rev. B **94**, 104522 (2016).
[46] Z. Liu, M. Chen, Y. Xiang, X. Chen, H. Yang, T. Liu, Q.-G. Mu, K. Zhao, Z.-A. Ren, and H.-H. Wen, Phys. Rev. B **100**, 094511 (2019).